ACS OMEGA

http://pubs.acs.org/journal/acsodf

Article

Compound-Specific 1D ^{1}H NMR Pulse Sequence Selection for Metabolomics Analyses

Upendra Singh, Shuruq Alsuhaymi, Ruba Al-Nemi, Abdul-Hamid Emwas,* and Mariusz Jaremko*

Cite This: *ACS Omega* 2023, 8, 23651−23663

Read Online

ACCESS | Metrics & More | Article Recommendations | Supporting Information

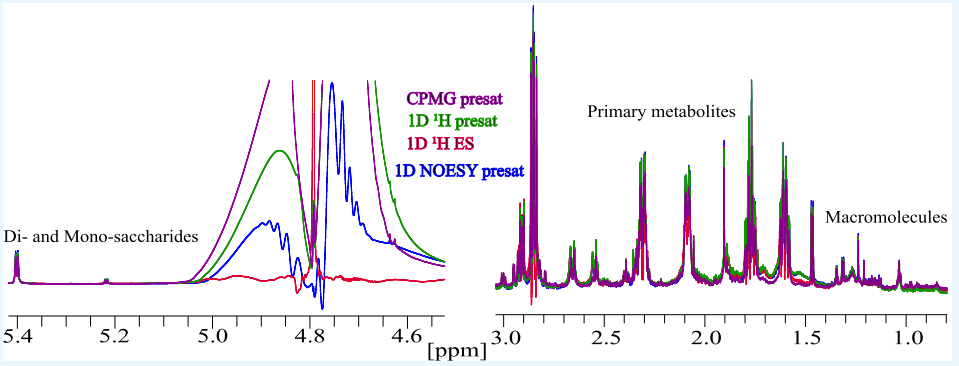

ABSTRACT: NMR-based metabolomics approaches have been used in a wide range of applications, for example, with medical, plant, and marine samples. One-dimensional (1D) ^{1}H NMR is routinely used to find out biomarkers in biofluids such as urine, blood plasma, and serum. To mimic biological conditions, most NMR studies have been carried out in an aqueous solution where the high intensity of the water peak is a major problem in obtaining a meaningful spectrum. Different methods have been used to suppress the water signal, including 1D Carr−Purcell−Meiboom−Gill (CPMG) presat, consisting of a T_2 filter to suppress macromolecule signals and reduce the humped curve in the spectrum. 1D nuclear Overhauser enhancement spectroscopy (NOESY) is another method for water suppression that is used routinely in plant samples with fewer macromolecules than in biofluid samples. Other common 1D ^{1}H NMR methods such as 1D ^{1}H presat and 1D ^{1}H ES have simple pulse sequences; their acquisition parameters can be set easily. The proton with presat has just one pulse and the presat block causes water suppression, while other 1D ^{1}H NMR methods including those mentioned above have more pulses. However, it is not well known in metabolomics studies because it is used only occasionally and in a few types of samples by metabolomics experts. Another effective method is excitation sculpting to suppress water. Herein, we evaluate the effect of method selection on signal intensities of commonly detected metabolites. Different classes of samples including biofluid, plant, and marine samples were investigated, and recommendations on the advantages and limitations of each method are presented.

INTRODUCTION

Metabolomics employs different analytical platforms such as high- or ultrahigh-performance liquid chromatography (UHPLC),[1] liquid chromatography coupled with mass spectrometry (LC−MS),[2−5] gas chromatography coupled to mass spectrometry (GC−MS),[3,6−8] and nuclear magnetic resonance (NMR) spectroscopy.[9−11] Among different analytical platforms, MS-based and NMR-based are the most used approaches in current metabolomics studies.[12−14] Although NMR spectroscopy has many advantages such as high reproducibility and minimal sample preparation, low sensitivity, and signal overlap are the main drawbacks of NMR compared to MS.[14,15]

One-dimensional (1D) ^{1}H NMR-based metabolomics studies utilize different methods to analyze metabolites in biological samples of plants, animals, humans, and marine organisms. These samples may include serum; plasma; urine; cell extracts; intestinal content; tissue;[16−27] plant seeds, flesh, leaves, stems, and roots;[28−34] and corals, algae, and jellyfish.[35−42] In high-resolution NMR spectroscopy, the focus is on the relational quantification of metabolites and estimation of metabolite concentrations in response to some perturbation. Metabolomics is used to observe relative quantitative changes and find out biomarkers.[43−49] Higher-dimensional NMR like pulse sequences of two-dimensional (2D) NMR is also used in metabolomics.[50−54] However, compared to a matching ^{1}H

Received: March 13, 2023
Accepted: April 13, 2023
Published: June 21, 2023

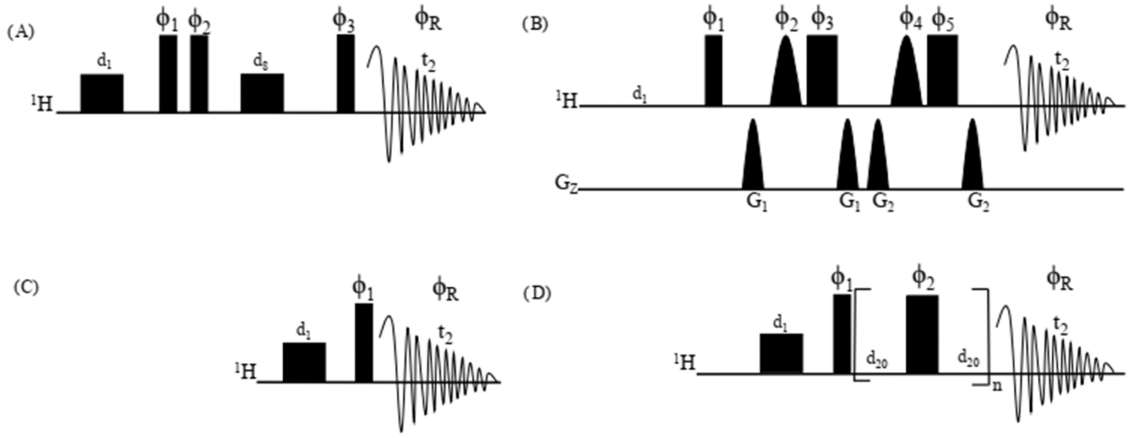

Figure 1. Pulse sequences of 1D ^{1}H NMR methods. (A) 1D NOESY presat, (B) 1D ^{1}H ES, (C) 1D ^{1}H presat, and (D) CPMG presat. Narrow and wide black-filled rectangles are 90 and 180° hard pulses, respectively, broad half-filled rectangles show presat of water resonance frequency during d_1, and half-black-filled sine shapes are soft 180° pulses used for water resonance frequency.[61] The d_1, d_8, d_{20}, and t_2 are relaxation delay, mixing time, half-spin-echo time, and acquisition time, respectively, and ϕ_1, ϕ_2, ϕ_3, ϕ_4, and ϕ_5 are phases of pulses, while ϕ_R is the phase of the receiver. G_1 and G_2 are pulse field gradients for the coherence transfer pathway.

NMR data set, 2D NMR data-processing time is significantly shorter because the signal overlap is not a significant issue and deconvolution is not necessary.[53]

Metabolomics is usually combined with multivariate statistical analyses such as principal component analysis (PCA), analysis of variance (ANOVA)-simultaneous component analysis (ASCA), and partial least squares-discriminant analysis (PLS-DA) chemometric methods.[55]

Preferred 1D methods for ^{1}H NMR-based metabolomics include 1D ^{1}H nuclear Overhauser effect spectroscopy (NOESY) presat pulse sequence, Carr−Purcell−Meiboom−Gill (CPMG) presat (T_2 filter),[56,57] 1D ^{1}H presat, and 1D ^{1}H excitation sculpting (ES) with gradients.[58] Despite the utility for 1D ^{1}H NMR of the first two methods, the pulse sequences of these methods have drawbacks.[59] Numerous pulse sequences have already been developed for water suppression, such as WET,[60,61] presaturation,[62] composite pulses,[63] WATERGATE,[64−66] or PURGE.[67] 1D NOESY presat pulse sequence (noesypr1d on Bruker spectrometers) has emerged as the preferred option for NMR-based metabolomics, because of its ability to significantly suppress the water signal. However, 1D NOESY presat does have a few drawbacks, including the inability to suppress signals of "faraway water" completely.[68]

A CPMG spin-echo sequence with presaturation is also a preferable 1D ^{1}H NMR-based metabolomics method, specifically for macromolecules like lipids, lipoproteins, and fat-bound lysis,[69] because of the incorporation of a T_2 filter into its pulse sequence (Figure 1). A T_2 filter in coupled spin systems is conventionally optimized to use very short interpulse spacing 2τ for spin-echo with a higher number of replications to filter out offsets of macromolecules and reduce the appearance of a humped curve in the high magnetic field region, which can cause severe sample heating, and suppresses the effects of slow chemical exchange processes.[70,71] This spin-echo causes transverse relaxation due to its large spacetime and also the self-diffusion of small molecules, resulting in a loss of sensitivity that is less considerable than the loss of sensitivity of macromolecules.[72−74] Another 1D ^{1}H NMR method with water suppression is a 1D ^{1}H pulse with excitation sculpting (ES),[58] which provides a spectrum with a well-suppressed water signal as well as pure phase spectra.[75] It consists of shape pulses and pulse field gradients, which cause artifacts and distortion in signals.[58,76−79] For nonaqueous solutions, 1D ^{1}H NMR experiment without presaturation (presat) of water is used routinely for chloroform extraction of nonpolar metabolites.[80] 1D ^{1}H NRM experiment with presat is also commonly used in the methanolic extraction of polar metabolites;[15,81−83] however, its spectrum suffers from humped curves in the methyl and methylene regions due to macromolecules like plasma and serum, caused by the absence of a T_2 filter like CPMG presat. In addition, enhancement in the sensitivity of these kinds of methods can be achieved by implementing spin-noise tuning optimum for salt and nonsalty samples.[84]

In this work, we evaluate and compare the effects of applied water suppression methods on the signal intensities of major metabolites classes. Moreover, we report a robust method providing highly reproducible spectra for compounds specifically in plasma, serum, plant flesh and seeds, and jellyfish (steroids, lipoproteins, terpenols, fatty acids, albumin-bound fatty acids, albumin lysis, primary metabolites, and mono- and disaccharides). The selection of pulse sequences is optimized to avoid dephasing and distortion in line shapes from an inappropriate relaxation rate and incomplete water suppression.

MATERIALS AND METHODS

Sample Preparation and Collection. For date palm samples, *Phoenix dactylifera* belonging to Anbara (Ar), Ajwa (AJ), Deglet Nour (DN), and Sukkaari (SR) dates were obtained from local farms in Medina and Qassim, Saudi Arabia, at the Tamar stage.

The plasma sample was purchased from Sigma-Aldrich (product no. H4522).

Fetal bovine serum (FBS) was purchased from Corning (product no. 35-010-CV).

For jellyfish samples, A *Cassiopea* (upside-down jellyfish) was collected from the red sea, SA. It dried for 24 h.

Metabolite Extraction. *Dates.* Following the protocol from ref 85, extractions of metabolites from the polar layer were carried out using methanol and LC-grade water. 100 mg of dried powder of each date type (fruit and seed) was homogenized in 1 mL of 80% methanol in water.[85] 800 μL of

https://doi.org/10.1021/acsomega.3c01688
ACS Omega 2023, 8, 23651−23663

Table 1. Experimental Acquisition and Processing Parameters

methods	NS	DS	SW (ppm)	AQ (s)	D1 (S)	mixing time (ms)	half-spin -echo time/loops	shape pulse/length	SI/LB	WDW
CPMG presat	128	4	20.1567	2	5		300 μs/120		131072/0.3 Hz	EM
1D NOESY presat	128	4	20.1567	2	5	100			131072/0.3 Hz	EM
1D ^{1}H ES	128	4	20.1567	2	5			Sinc/2 ms	131072/0.3 Hz	EM
1D ^{1}H presat	128	4	20.1567	2	5				131072/0.3 Hz	EM

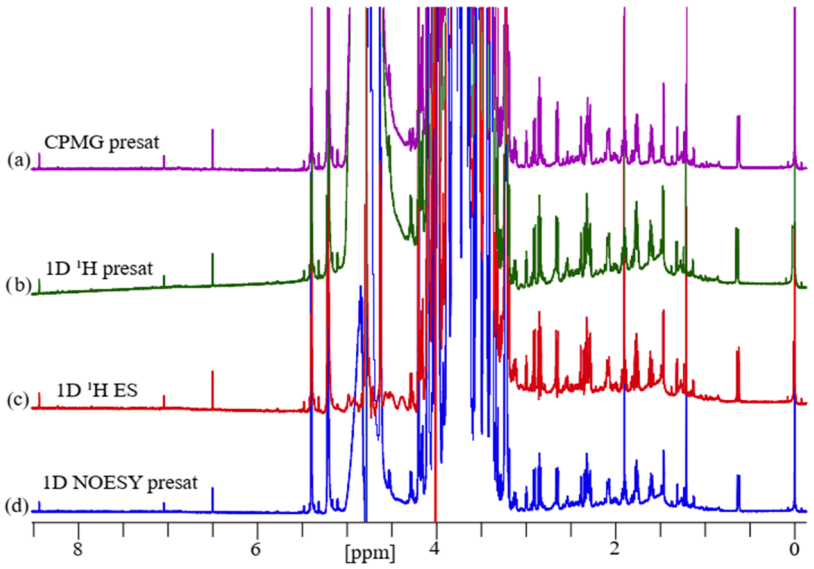

Figure 2. Comparative 1D ^{1}H NMR spectra of different 1D ^{1}H NMR methods. The spectra show palm date flesh with each method differentiated by color: 1D NOESY presat (d, blue), 1D ^{1}H ES (c, red), 1D ^{1}H presat (b, green), and CPMG presat (a, purple).

the polar sample was dried in a CentriVap concentrator (Labconco), without heating, and stored at −20 °C for the NMR analysis.

^{1}H NMR Sample Preparation. *Date Palms Fruits and Seeds.* Samples were prepared by dissolving the pellets in 400 μL of D_2O and 200 μL of potassium phosphate buffer (K + buffer) of concentration 20 mM and pH 7.4 in 1.5 mL Eppendorf tubes. The samples were vortexed until they dissolved completely and then centrifuged at 13,000 rpm for 5 min, and 500 μL was transferred into 5 mm NMR tubes.

Methanol-Extracted FBS and Plasma. 200 μL of serum or plasma was dissolved in 400 μL of methanol, vortexed for 30 s and then incubated at −20 °C for 20 min, followed by centrifugation for 30 min at 4 °C, 12,000 rpm. The supernatant (500 μL) was dried for 12 h till fully dried. Then, the pellet dissolved in 300 μL of D_2O and 300 μL of potassium phosphate buffer (20 mM and pH of 7.4) and was centrifuged for 10 min, at 4 °C, 12,000 rpm. 500 μL of supernatant was transferred into an NMR tube.

Fetal Bovine Serum (FBS). 200 μL of serum was dissolved in 400 μL of K+ potassium phosphate buffer (20 mM and pH of 7.4) and vortexed for 30 s, followed by centrifugation for 10 min at 4 °C, 12,000 rpm. The supernatant (500 μL) was taken for NMR analysis.

Jellyfish. 50 mg was dissolved in 1 mL of So1 (MeOH/H_2O, 80:20) and vortexed for 10 min. It was homogenized by shaking at 4 °C for 90 min at 14,000 rpm and centrifuged at 13,000 rpm for 5 min to collect the supernatant to be lyophilized to obtain pellets. Pellets were dissolved in 300 μL of D_2O and 300 μL of K + potassium phosphate buffer (20 mM and pH of 7.4) and centrifuged for 10 min at 4 °C, 12,000 rpm. 500 μL of supernatant was transferred into an NMR tube.

^{1}H NMR Experiments and Processing Parameters for All 1D ^{1}H NMR Experiments. A Bruker 800 MHz AVANACE NEO NMR spectrometer equipped with Bruker TCI (^{1}H/^{13}C/^{15}N) cryogenic probe (Bruker BioSpin, Rheinstetten, Germany) was used to record all NMR spectra at 298 K. Transformed spectra were processed for phase and baseline distortions using Topspin 4.0.7 (Bruker BioSpin) and then automatically calibrated to the proton signal of DSS at 0.00 ppm. The applied acquisition and processing parameters for all 1D ^{1}H methods were shown in Table 1.

RESULTS AND DISCUSSION

For Palm Anbara Date Flesh and Its Seeds (*P. dactylifera*). Among several applied methods, a few 1D ^{1}H NMR spectra from different experiments were collected to find the highest signal-to-noise ratio (SNR) and phased signals without artifacts over the same acquisition and processing parameters for a few samples belonging to plants, biofluids, and marine. The pulse sequences of four selected methods which are common in metabolomics are shown in Figure 1.

1D ^{1}H NMR spectra were depicted in different colors in Figure 2, showing 1D ^{1}H presat (green), 1D NOESY presat (blue), 1D ^{1}H ES (red), and CPMG presat (purple). 1D ^{1}H ES (red) shows gradient imperfections and partial evolution of scalar coupling due to shape pulses with long pulse lengths compared to hard pulses and pulse field gradients with long pulse lengths.[58] This causes line-shape distortions, as shown enclosed in the green box in Figure 2, while other methods do not have such shape distortions since they do not have pulse field gradients. Qualitative and quantitative analyses of signals in the spectra were performed in the extended sections from

https://doi.org/10.1021/acsomega.3c01688
ACS Omega 2023, 8, 23651−23663

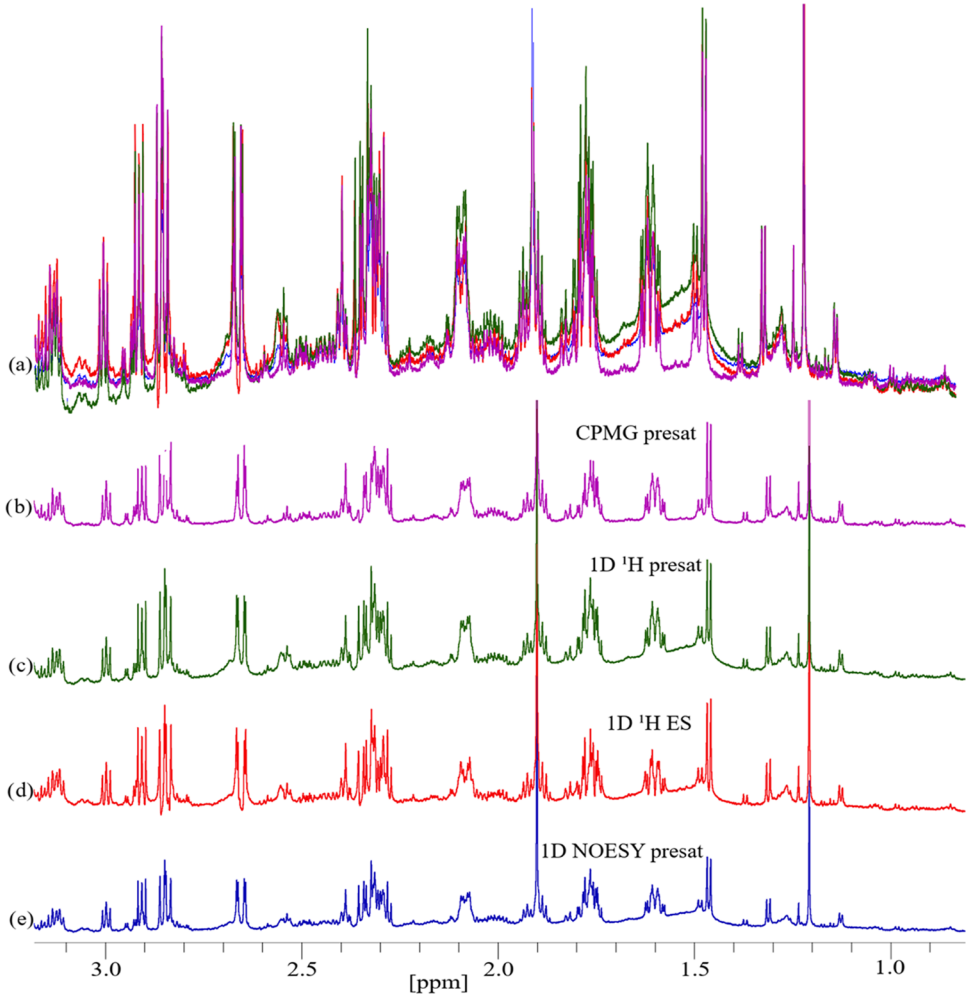

Figure 3. Comparative 1D ^{1}H spectra of different 1D ^{1}H NMR methods. (a) Overlapping spectra from all experiments with their colors as mentioned above: (b) CPMG presat, (c) 1D ^{1}H presat, (d) 1D ^{1}H ES, and (e) 1D NOESY presat. Extended sections from 0.79 to 3.15 ppm are shown in all plots, measuring palm anbara date flesh.

0.79 to 3.15 ppm in toggled mode with overlapped spectra (Figure 3). Normalization of signal-to-noise ratios of normal protons with presat was performed to compare with the most common 1D proton methods used routinely in metabolomics. Distortions were present in line shapes at chemical shifts of 1.31(d), 1.60(m), 1.76(m), 2.34(m), 2.65(dd), 2.85(m), 2.90(m), and 3.00(t). Figure 3 shows carbohydrate signals with less distortion than signals in the higher-magnetic-field region. Figure 4 shows the effect of a gradient on shape distortion, proportional to the strength of the applied external magnetic field in 1D ^{1}H ES. There is no such effect in the other three methods. These effects mean that measurement of the area under the signal is imperfect, therefore showing the unsuitability of the 1D ^{1}H ES method for metabolomics in palm anbara date flesh samples. The signal-to-noise ratio (SNR) values of metabolites obtained from these four 1D ^{1}H NMR experiments have been calculated manually and are shown in Table S1. The formula for finding the increment and decrement in percentages are given below in Table S1.

The SNR of this 1D ^{1}H ES method was compared with the normal proton with the presat (normalized) method. This showed a general reduction of signal, which was 10% for steroids, 0% for terpenols, 4% for fatty acids, 1% for primary metabolites, 44% for α-glucose, 96% for β-glucose, and 6% for sucrose, as shown in Table S2. The SNR was close to CPMG presat for all metabolite types but lower by 42 and 84% for α-glucose and β-glucose, respectively. For disaccharides, it was the same but around 40% higher than 1D NOESY presat and not the same as carbohydrates as shown in Table S2. Robustness was measured by taking an average of SNR values in Table S1 for selective kinds of metabolites. The shape pulses have excited the near signals close to the water signal, which resulted in the suppression of the close signals to the resonance frequency of water. The singlet signals have higher SNR values than 1D ^{1}H presat by 10% (Table S1). The CPMG with presat spectra provided more flattened baselines in the methyl and methylene regions compared to other samples, with non-distorted line shapes like 1D ^{1}H presat and 1D NOESY presat. The SNR values of these signals were measured with an overlapping baseline. SNR values in the CPMG presat spectrum were abnormal in the case of a few metabolites like steroids, α-glucose, β-glucose, and sucrose with values that were 90, 96, 86, and 94% of 1D ^{1}H presat SNR normalized values, respectively. For fatty acids and primary metabolites, there was no significant variation (Table S2).

In contrast and unexpectedly, we found a significant loss in the SNR of 1D NOESY presat, which was around 35% for most of the metabolites, 44% for steroids, and 51% for β-

https://doi.org/10.1021/acsomega.3c01688
ACS Omega 2023, 8, 23651−23663

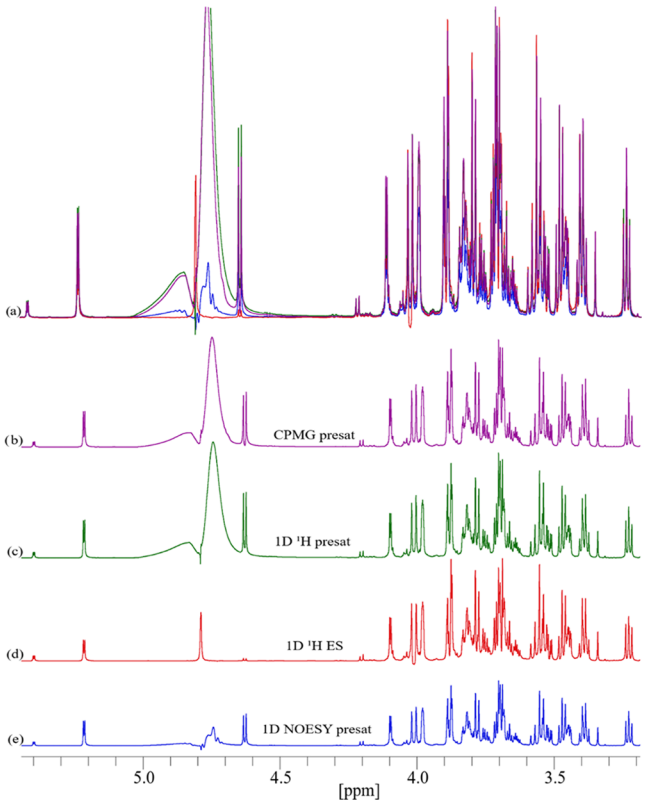

Figure 4. Extended 1D ^{1}H NMR spectra of palm anbara date flesh from 3.25 to 5.45 ppm. (a) Overlapped spectra with colors representing abovementioned different 1D ^{1}H NMR methods and their toggled forms from (b−e).

glucose for a signal at 4.63 ppm (Table S2). Therefore, we recorded for the same palm anbara date flesh and another type of palm sukkari date flesh to check its reproducibility, as shown in Figures S3 and S4. The results were similar to Table S2 results. The plant flesh was palm anbara date flesh consisted of minerals in the form of metal ions,[86,87] resulting in increased conductivity, which caused inhomogeneity in the magnetic field and affected the optimized pulse length of the ^{1}H hard 90° pulse because it is more sensitive to the ionic effect. Electrical noise produced by conductive substances can significantly lower the sensitivity of NMR probes. A high salt concentration has an impact on tuning, matching, and probe performance. High ionic strength impacts T_1 relaxation and 90° pulses (particularly in ^{1}H).[88]

In the case of seeds from the same palm anbara date flesh, the result was quite different in SNR values of 1D NOESY presat compared to 1D ^{1}H presat (Table S8). Increments in SNR values for primary metabolites, fatty acids, α-glucose, β-glucose, and sucrose were found to be 6, 4, 7, 7, and 3% respectively, while for others, they were the same, without any line-shape distortions as shown in Figures S5−S7. 1D ^{1}H ES had different SNR values resulting in losses of 10% for steroids, 4% for fatty acids, 5% for primary metabolites, and 48% for α-glucose. The β-glucose signal at 4.60 ppm was completely suppressed, and the sucrose signal increased by 6%. The SNR value for terpenols (Table S9) was similar to line-shape distortions in a few signals as shown in Figure S6. The spectrum of CPMG with presat was like palm anbara date flesh with a flattened baseline, without distortions in the line shapes (Figures S5−S7), but a significant reduction in the SNR values was found, by 10% for steroids, 14% for β-glucose, and 6% for sucrose, while insignificant for others (Table S9).

Methanol-Extracted Plasma Samples in Which the Macromolecule (Lipoproteins, Steroids, Albumin−Fatty Acid) Precipitate Is Filtered Out by Methanol. Figure 5 shows all overlapping 1D ^{1}H NMR spectra of methanol-extracted plasma. The baselines were not flat due to a higher concentration of different types of macromolecules (Table S12), which causes a humped curve inside the signals (with the exception of CPMG presat). The line shapes of these spectra were analyzed qualitatively in the extended portions from 0.75 to 3.01 ppm along with the toggled form of these spectra shown in Figure 6 and other extended portions from 3.02 to 5.45 ppm and from 5.30 to 8.6 ppm in Figures S10 and S11. Distortion in the shape of a few lines of multiplets was found in the 1D ^{1}H ES spectrum at chemical shifts of ppm 0.95(m), 1.31(d), 1.46(d), 1.75(m), 2.90(m), and 3.70(m), shown in Figures 6 and 7 in red. SNR values were found to be like 1D ^{1}H presat in the methyl region, 10 and 4% higher for lipoprotein and albumin-bound fatty acids in the methylene region, respectively. Overall, the SNR values for categorized molecules were like 1D ^{1}H presat, 1D NOESY presat, and

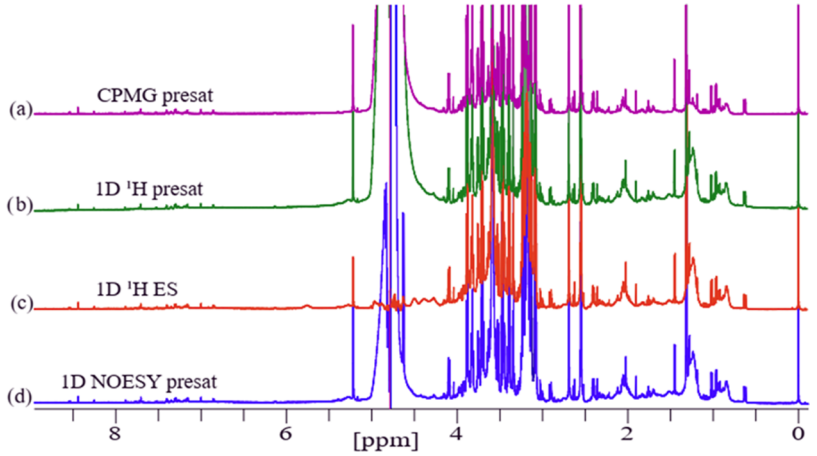

Figure 5. Overlapped plasma (methanol extract) 1D ^{1}H NMR spectra with different 1D NMR methods distinguished by color: 1D NOESY presat (d, blue), 1D ^{1}H ES (c, red), 1D ^{1}H presat (b, green), and CPMG presat (a, purple).

https://doi.org/10.1021/acsomega.3c01688
ACS Omega 2023, 8, 23651−23663

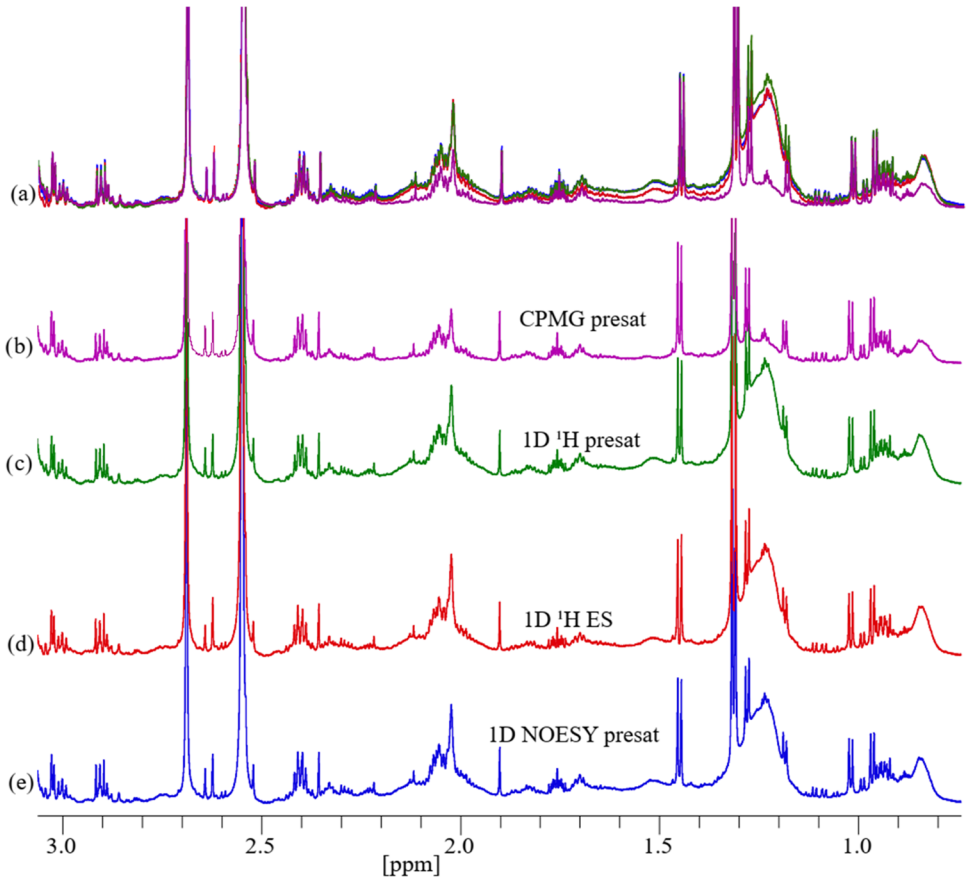

Figure 6. Displays extended sections from 0.79 to 3.15 ppm of the overlapped (a) and toggled 1D ^{1}H NMR spectra of different 1D NMR methods with their colors as mentioned in above overlapped 1D ^{1}H spectra of CPMG presat (purple, b), 1D ^{1}H presat (green, c), 1D ^{1}H ES (red, d), and 1D NOESY presat (blue, e) of the plasma (methanol extract) sample.

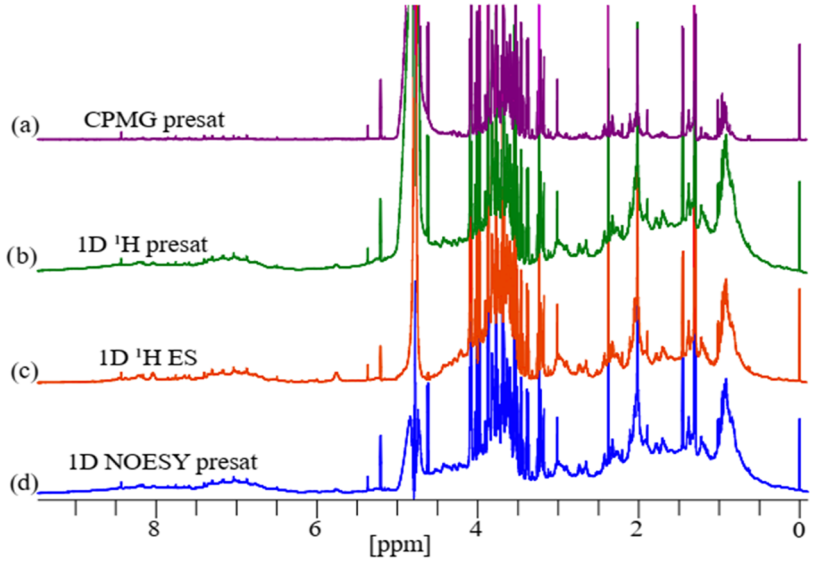

Figure 7. Overlapping serum (non-methanol extract) 1D ^{1}H NMR spectra of different 1D NMR methods. Colors are 1D NOESY presat (d, blue), 1D ^{1}H ES (c, red), 1D ^{1}H presat (b, green), and CPMG presat (a, purple).

CPMG presat for steroids and lipoproteins, while no significant change in values was present for albumin-bound fatty acids.

Primary metabolites increased by 3 and 4% respectively and had an increase of 7−12% for singlet signals from higher- to lower-magnetic-field regions. There was also a large reduction of about 46 and 98% for α-glucose and β-glucose (Table S13), respectively, and an increase of 12% in multiplets of glucose (Table S12) with a humped curve in the methyl and methylene regions. The 1D NOESY presat spectrum had SNR values mostly equal to 1D ^{1}H presat; however, the signals of a few metabolites increased by a minimum of 3% for multiplets and a maximum of 10% for singlet signals (Table S12). Overall, there

https://doi.org/10.1021/acsomega.3c01688
ACS Omega 2023, 8, 23651−23663

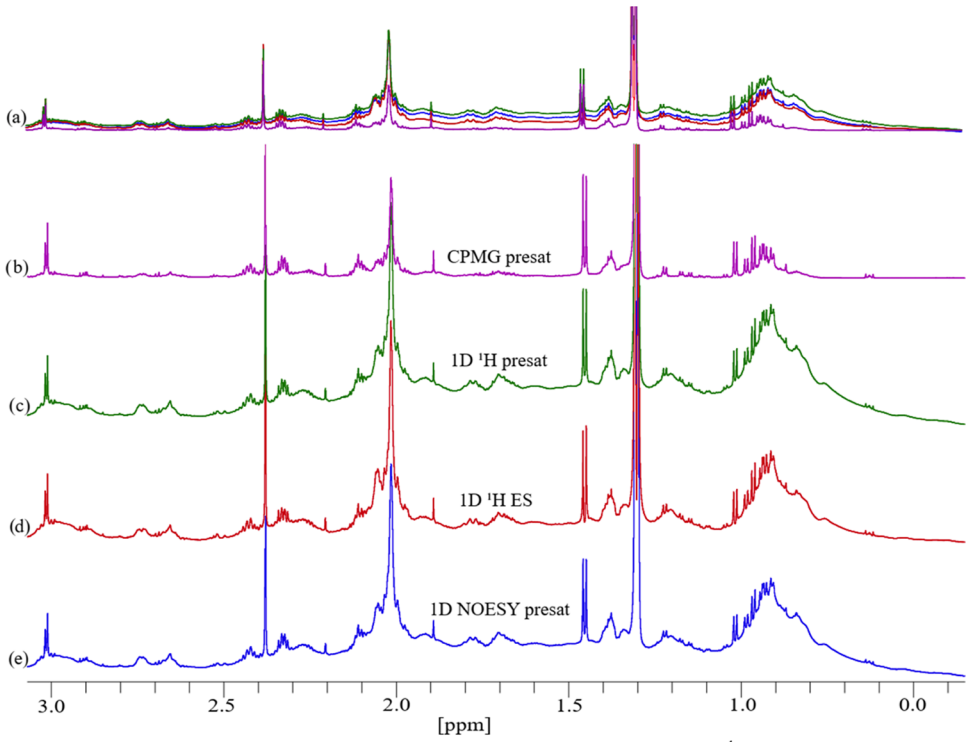

Figure 8. Extended sections of fetal bovine serum (FBS) (non-methanol extract) 1D ^{1}H NMR spectra from 0.79 to 3.15 ppm, with overlapped (a) and toggled 1D ^{1}H NMR methods denoted by colors: CPMG presat (purple, b), 1D ^{1}H presat (green, c), 1D ^{1}H ES (red, d), and 1D NOESY presat (blue, e).

was an increased percentage in SNR, 3% for primary metabolites, 2% for lipoproteins, and 7% for β-glucose, while other signals had equal values (Table S13) with the same humped curve in the methyl and methylene regions. This humped curves under the signals were suppressed in the spectrum of CPMG presat shown in Figure 6b and the rest of the extended portions in Figures S10 and S11 as well as having equal SNR values for steroids, lipoproteins but decreased of 13% for albumin-bound fatty acids, and the most important result is the increment of 4% for primary metabolites and decrement of 5% for both α-glucose and β-glucose.

Non-Methanol-Extracted Fetal Bovine Serum (FBS). Figure 7 shows overlapping 1D ^{1}H NMR spectra of methanol-extracted serum samples. The baseline of all experiments except CPMG presat was not flat due to a higher concentration of different types of macromolecules, categorized into groups of molecules (Table S15).

An extended portion of the 1D ^{1}H NMR spectra from 0.79 to 3.15 ppm from all experiments is shown in Figure 8, with 3.15−8.65 ppm in Figure S14. The nonextracted serum contains macromolecules in higher concentrations, which causes the humped curve in the baseline shapes of all spectra except CPMG presat. SNR values of signals from all ^{1}H 1D NMR experiments were analyzed, and CPMG presat had SNR values close to 1D ^{1}H presat and 1D ^{1}H ES but higher by 10% compared to 1D NOESY presat.

An extended portion of the 1D ^{1}H NMR spectra from 0.79 to 3.15 ppm from all experiments is shown in Figure 8, with 3.15−8.65 ppm in Figure S14. The nonextracted serum contains macromolecules in higher concentrations, which causes the humped curve in the baseline shapes of all spectra except CPMG presat. SNR values of signals from all ^{1}H 1D NMR experiments were analyzed, and CPMG presat had SNR values close to 1D ^{1}H presat and 1D ^{1}H ES but higher by 10% compared to 1D NOESY presat.

Finally, there was a decrease in steroids by 23%, terpenols by 9%, lipoproteins by 11%, albumin-bound fatty acids by 12%, albumin lysis by 11%, primary metabolites by 9%, α-glucose by 11%, and β-glucose by 14%. However, fetal bovine serum (FBS) that was methanol-extracted to filter out precipitates of macromolecules had a different ratio of SNR values and had insignificant humped curves under the signals in the methyl regions of all spectra as shown in Figure S17. 1D ^{1}H presat showed the highest humped curve under its signals but the highest sensitivity, while CPMG presat showed the highest flattened baseline but the lowest signal sensitivity. The reduction of sensitivity in the CPMG presat spectrum was a decrease of 3−5% for multiplets and an exceptional 2% for doublets of lactate compared to 1D ^{1}H presat shown in Table S16. 1D NOESY presat and 1D ^{1}H ES showed sensitivity like CPMG presat and had a higher humped curve than CPMG presat. Overall, 1D ^{1}H presat and CPMG presat were robust for fetal bovine serum (FBS), both methanol- and non-methanol-extracted.

Jellyfish (*Cassiopea*). The full overlapped 1D ^{1}H NMR spectra of all experiments presented the insignificant humped curves in all of the 1D ^{1}H NMR spectra (Figure S18), while 1D NOESY presat provided the lowest SNR values compared to others, but CPMG presat with the highest flat baseline of shapes of its spectrum in methyl and methylene regions resulted in SNR values close to 1D ^{1}H presat. The 1D ^{1}H presat spectrum had the highest SNR values overall as shown in Figures S19−S21. A significant reduction in the SNR values was present for 1D ^{1}H ES, close to 10% compared to 1D ^{1}H presat (Table S22). 1D ^{1}H ES had no steroid and fatty acid signal, a reduction of 10% for terpenols and sucrose, 8% for

https://doi.org/10.1021/acsomega.3c01688
ACS Omega 2023, 8, 23651−23663

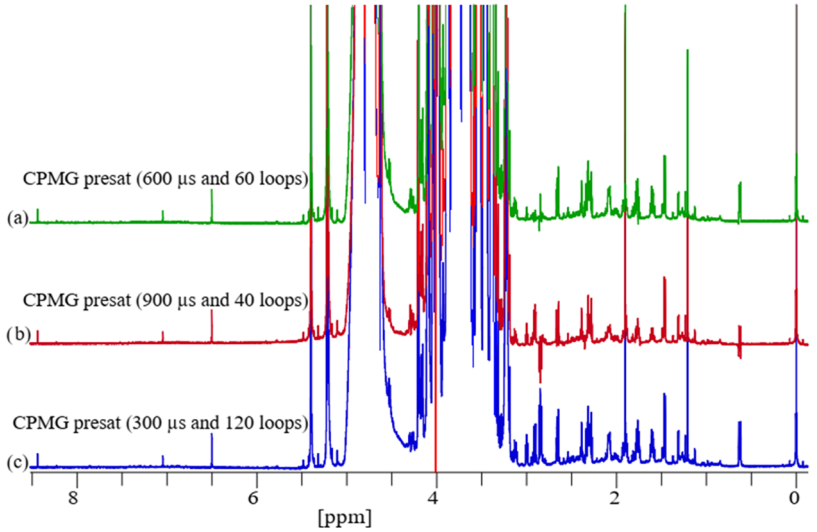

Figure 9. Full overlapped 1D ^{1}H NMR spectra of palm anbara date flesh, showing CPMG presat (c, blue) with half-spin-echo time and number of loops of 300 μs and 120, CPMG presat (b, red) with 900 μs and 40, CPMG presat (a, green) with 600 μs and 60, respectively. The red spectrum showed a more dephased signal than the others.

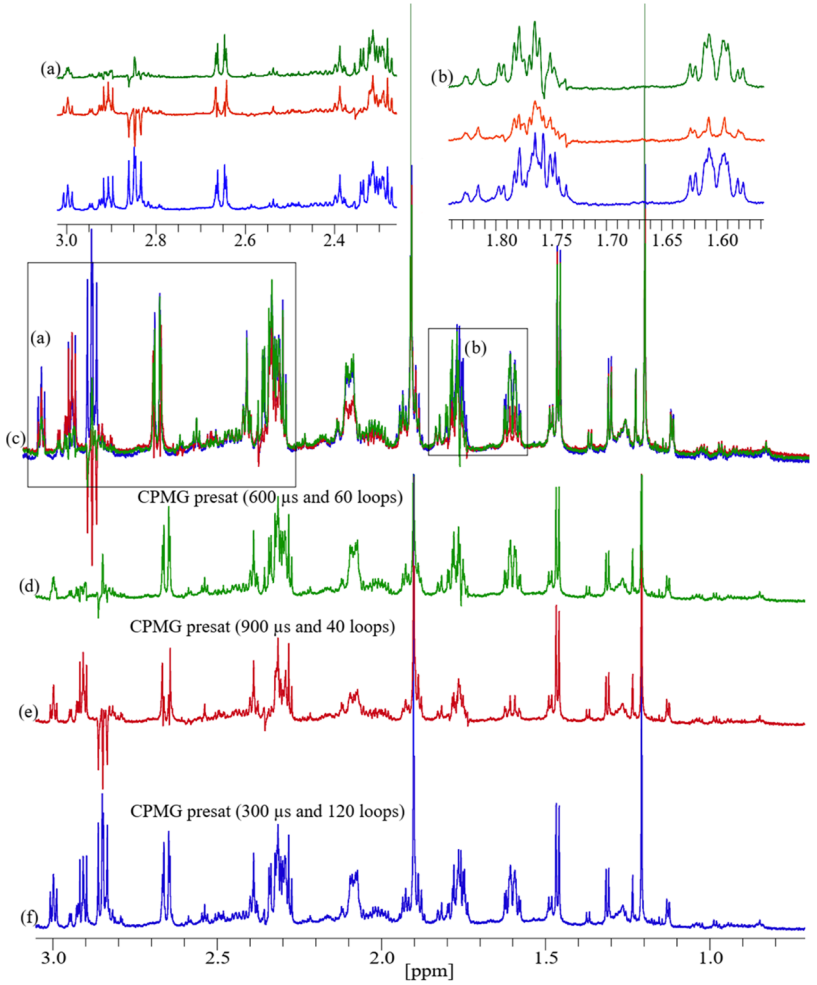

Figure 10. Extended portions of 1D ^{1}H NMR spectra from 0.71 to 3.05 ppm of overlapped spectra (c) with (a, b) extended section of its few parts of experiments of CPMG presat (green, d) with half-spin-echo time and number of loops of 600 μs and 60, CPMG presat (red, e) with 900 μs and 40, CPMG presat (blue, f) with 300 μs and 120, respectively, top of overlapped spectra of all for palm anbara date flesh samples. The red spectrum had more distortions in quantity and quality than green, while blue did not have any distortions compared to those but had higher sensitivity of signals than signals of red and green spectra. The reduction in sensitivities of the red spectrum is higher than that of the blue and green spectra.

https://doi.org/10.1021/acsomega.3c01688
ACS Omega 2023, 8, 23651−23663

primary metabolites, 24% for α-glucose, and 63% for a β-glucose at 4.60 ppm (Table S23). There was an increase in lipoproteins by 2% compared to the 1D ^{1}H presat spectrum. This table also shows a decrease in the SNR of CPMG presat for lipoproteins (5%), terpenols (10%), primary metabolites (7%), sucrose (6%), and α-glucose and β-glucose (2 and 5%, respectively) compared to 1D ^{1}H presat. Similarly, there was a significant reduction in the SNR for all molecules in 1D NOESY presat (Table S22). Overall, there was a complete disappearance of steroids and fatty acids compared to 1D ^{1}H presat, while other signals were reduced (terpenols: 27%, lipoproteins: 17%, primary metabolites: 11%, sucrose: 10%, α-glucose: 5%, and β-glucose: 8%) (Table S23). SNR values obtained from 1D ^{1}H ES and 1D NOESY presat showed a significant reduction compared to 1D ^{1}H presat and no significant reduction in carbohydrates and primary metabolites in CPMG presat compared to zgpr. The robustness of the 1D ^{1}H presat method dominated the rest of the experiments for jellyfish (*Cassiopea*).

Comparison of CPMG Presat with Different Half-Spin-Echo Times and the Number of Loops. *For the Palm Anbara Date Flesh.* Varying half-spin-echo times and number of loops for CPMG presat altered the phase of a few signals (Figure 9). For a clear vision of signal line shapes, overlapped spectra are shown from 0.7 to 3.05 ppm, from 1.55 to 1.84 ppm, and from 2.25 to 3.00 ppm (Figure 10). The remaining extended sections from 3.00 to 4.65 and 5.10 to 8.50 ppm with the extended region from 5.10 to 5.41 ppm are shown in Figures S24 and S25, respectively. For CPMG presat with a half-spin-echo time of 900 μs and loops of 40, there was a significant decrement in the sensitivity, with dephased signals in the spectrum (red). This is due to the longer half-spin-echo time, which causes evolution under scalar coupling (mismatching J-coupling values) of small molecules. It also results in dephased signals, and transverse relaxation results in a reduction of sensitivity compared to a smaller time (300 μs and 120, blue). A smaller number of loops also cause less heating of the sample. Spectra from 600 μs half-spin-echo time and 60 loops caused less evolution under scalar coupling of the small molecules compared to the spectrum from 900 μs half-spin-echo time. Therefore, reduction of sensitivity and dephasing of signals was less than for the spectrum from longer half-spin-echo as discussed above. Overall, there was a reduction of sensitivity by 27 and 7% in red and green spectra, respectively, compared to smaller half-spin-echo time (300 μs) and 120 larger loops. This showed the robustness of using smaller values for half-spin-echo time for CPMG presat for primary metabolites in palm anbara date flesh.

Palm Anbara Date Seeds. Figure S26 compares CPMG presat with different half-spin-echo times and loop numbers. The same dephased and distorted signals are seen as in the palm date flesh. Similarly, the extended portions of the spectra from 0.71 to 3.05 ppm (Figure S27), 3.01 to 4.65 ppm (Figure S28), and 5.10 to 8.50 ppm (Figure S29) are seen. Palm anbara date seeds showed similar trends as the flesh. Suitable acquisition parameters for half-spin-echo and the number of loops for CPMG presat are also 300 μs and 120, respectively.

For the Sample of Plasma (Methanol-Extracted). The full overlapped spectra of CPMG presat with different values of half-spin-echo times and number of loops showed dephasing of a few signals, and suppression of macromolecules was obtained identical for each different times and loops, while dephasing and distortions in line shapes were also observed (Figure S30). The extended portion from 0.78 to 3.00 ppm showed higher dephasing and reduction of sensitivity in the green (600 μs and 60 loops) spectrum compared to the rest of the spectra. The sensitivity of the signals in the blue (300 μs and 120 loops) spectrum without any dephasing was higher than that of the red and green spectra (Figure S31). The other extended portions from 3.0 to 4.65 and 5.10 to 8.50 ppm are shown in Figures S32 and S33, respectively. In the lower-magnetic-field region, the shape and sensitivities of lines in the spectra were similar and equal, except for the signal at 4.10 ppm (q), which was dephased and close to being suppressed in the green spectrum. The spectral quality and sensitivity of the blue spectrum (300 μs and 120 loops) dominated over the red and green spectra.

Non-Methanol-Extracted Fetal Bovine Serum. The full overlapped spectra of CPMG presat with different values of half-spin-echo times and the number of loops showed dephasing and reduction of sensitivity in a few signals at 2.90 (m) and 4.10 (q) ppm in the green spectrum (Figure S34). The extended portions from 0.71 to 3.05 ppm, from 3.0 to 4.65 ppm, and from 5.10 to 8.50 ppm are shown in Figures S35−S37, respectively. Similarity in the shapes and sensitivities of signals as in the plasma sample indicated the suitability of the blue spectrum (300 μs and 120 loops) for non-methanol-extracted fetal bovine serum.

Finally, the proton with presat (1D ^{1}H presat) is a robust method for the samples of plant fleshes and methanol-extracted plasma and fetal bovine serum, and jellyfish (Table S38 and Bar Chart S39), 1D NOESY presat for plant date seeds, and CPMG presat is better for non-methanol-extracted plasma and serum. For this observation, we have shown (Table S40) the application of 1D ^{1}H NMR methods in previous studies for biological, plant, and marine samples in ratios as 29% of CPMG presat for mostly serum and plasma samples, 39% of 1D NOESY presat for mostly urine and plant samples, 14% of 1D ^{1}H ES for all types of samples, and 18% of 1D ^{1}H presat for all types of samples but mostly urine and plant samples shown in Pie Chart S41.

The maximum T_1 values of all molecules of that sample should be used for full longitudinal relaxation of all magnetizations for quantification of primary metabolites by 1D ^{1}H NMR. Therefore, we have measured the maximum range of T_1 values of all molecules of sukkari palm date flesh, plasma, fetal bovine serum, and jellyfish samples. We have shown the 1D ^{1}H spectra for T_1 measurements for palm date flesh in Figures S42 and S43, plasma (methanol-extracted) in Figure S44, and fetal bovine serum (methanol-extracted) in Figure S45. The maximum T_1 values of all molecules of these samples are presented in Table S46 where 3.0 and 5.0 s for singlet and multiplet signals, respectively, for palm date flesh, plasma, and fetal bovine serum, which are higher than 3 and 5 times relaxation delays, respectively, are used in the four different 1D ^{1}H NMR experiments for comparative quantification of metabolites in the metabolomics. Our given relaxation delay and acquisition time are suitable for comparative quantification like metabolomic profiling, and accordingly measured T_1 values show the required relaxation delay between 15 and 25 s for absolute quantification. Our study focused on comparison of methods for comparative quantification as metabolomics with a suitable 1D ^{1}H NMR method, which followed the acquisition parameters from reported journal for the protocol of metabolomics.[16,17]

https://doi.org/10.1021/acsomega.3c01688
ACS Omega 2023, 8, 23651−23663

CONCLUSIONS

In summary, comparative analysis of the spectra from different 1D ^{1}H NMR methods resulted in the selection of a method specific to the samples. For anbara palm date-flesh, the 1D ^{1}H presat spectrum is the best and 1D NOESY presat is the worst, being highly sensitive to ionic effects in the solution. For seeds of the same anbara palm dates, the spectrum of 1D NOESY presat is a little better in comparison to 1D ^{1}H presat and the other two methods. In the case of plasma (methanol-extracted), all methods showed similar SNR values with insignificant reduction, incrementation, and no distortion or dephased signals, except for small levels of the humped curve in the methyl region. CPMG presat shows its robustness with the best flat baselines in its spectrum for fetal bovine serum (non-methanol-extracted) as well as an insignificant reduction in SNR values to 1D ^{1}H presat. However, the overall SNR values of the 1D ^{1}H presat spectrum show that it is a robust method for fetal bovine serum in methanol-extracted samples. The 1D ^{1}H presat spectrum provided SNR values greater than those of 1D NOESY presat, 1D ^{1}H ES, and CPMG presat. 1D ^{1}H presat is robust over other methods for jellyfish samples. 1D ^{1}H presat has high and uniform SNR values for all metabolites because it does not have extra pulse sequences like the T_2 filter in CPMG presat, mixing pulse in 1D NOESY presat, and shape pulses and gradients in 1D ^{1}H ES, which cause different levels of fluctuations in the values of SNR for different types of signals like singlet, doublet, and multiplet due to the evolution of magnetizations under scalar couplings, unwanted coherence transfer among magnetizations, dephasing by gradients, and excitation of nearby magnetizations to water magnetization. Overall, the proton with presat (1D ^{1}H presat) is a robust method for samples of plant fleshes, methanol-extracted plasma, and fetal bovine serum, and jellyfish, 1D NOESY presat for plant palm date seeds, and CPMG presat is better for non-methanol-extracted plasma and serum with appropriate acquisition parameters for metabolomics. The CPMG presat method suppresses macromolecule signals in the methyl and methylene regions by applying a T_2 filter, which depends on half-spin-echo time and the number of loops. A half-spin-echo time of 300 μs and 120 loops are more appropriate for suppressing signals of macromolecules than the half-spin-echo times of 900 μs with 40 loops and 600 μs with 60 loops because this lowest time and highest loops values cause CPMG presat to avoid a humped under curve area of signals without dephasing or reducing the sensitivity of signals in the spectrum than rest of the values of half-spin-echo time and the number of loops.

ASSOCIATED CONTENT

Supporting Information

The Supporting Information is available free of charge at https://pubs.acs.org/doi/10.1021/acsomega.3c01688.

(i) 1D ^{1}H NMR spectral signal-to-noise ratio values tables for all samples; (ii) 1D ^{1}H overlapping NMR spectra with different methods for all samples; (iii) 1D ^{1}H NMR spectra comparisons of different half-spin-echo times and the number of loops for CPMG presat for all samples; (iv) bar chart showing increases or decreases in SNR of the spectra for different methods and specific compounds; (v) 1D ^{1}H NMR methods used in the literature as a table; (vi) pie chart showing % of 1D ^{1}H methods used in metabolomics studies for biological, plant, and marine samples; (vii) 1D ^{1}H NMR spectra showing T_1 measurements for all samples; and (viii) table showing T_1 values of signals for all samples (PDF)

AUTHOR INFORMATION

Corresponding Authors

Abdul-Hamid Emwas − *Core Lab of NMR, King Abdullah University of Science and Technology (KAUST), Thuwal, Makkah 23955-6900, Saudi Arabia*; Email: abdelhamid.emwas@kaust.edu.sa

Mariusz Jaremko − *Smart-Health Initiative (SHI) and Red Sea Research Center (RSRC), Division of Biological and Environmental Sciences and Engineering (BESE), King Abdullah University of Science and Technology (KAUST), Thuwal, Makkah 23955-6900, Saudi Arabia*; Email: mariusz.jaremko@kaust.edu.sa

Authors

Upendra Singh − *Smart-Health Initiative (SHI) and Red Sea Research Center (RSRC), Division of Biological and Environmental Sciences and Engineering (BESE), King Abdullah University of Science and Technology (KAUST), Thuwal, Makkah 23955-6900, Saudi Arabia*; orcid.org/0000-0002-9231-3850

Shuruq Alsuhaymi − *Smart-Health Initiative (SHI) and Red Sea Research Center (RSRC), Division of Biological and Environmental Sciences and Engineering (BESE), King Abdullah University of Science and Technology (KAUST), Thuwal, Makkah 23955-6900, Saudi Arabia*

Ruba Al-Nemi − *Smart-Health Initiative (SHI) and Red Sea Research Center (RSRC), Division of Biological and Environmental Sciences and Engineering (BESE), King Abdullah University of Science and Technology (KAUST), Thuwal, Makkah 23955-6900, Saudi Arabia*; orcid.org/0000-0002-1288-6916

Complete contact information is available at: https://pubs.acs.org/10.1021/acsomega.3c01688

Notes

The authors declare no competing financial interest.

ACKNOWLEDGMENTS

The authors would like to thank King Abdullah University of Science and Technology (KAUST) for financial support. Smart Health Initiative (SHI) is also acknowledged by M.J. for the grants financed with the source of Baseline (BAS/1/1085-01-01) in the period of 2021−2023.

REFERENCES

(1) de Souza, L. P.; Alseekh, S.; Scossa, F.; Fernie, A. R. Ultra-high-performance liquid chromatography high-resolution mass spectrometry variants for metabolomics research, Nature Methods. *Nat. Methods* **2021**, *18*, 733−746.

(2) Zhu, G.; Wang, S.; Huang, Z.; Zhang, S.; Liao, Q.; Zhang, C.; Lin, T.; Qin; Peng, M.; Yang, C.; Cao, X.; Han, X.; Wang, X.; van der Knaap, E.; Zhang, Z.; Cui, X.; Klee, H.; Fernie, A. R.; Luo, J.; Huang, S. Rewiring of the fruit metabolome in tomato breeding. *Cell* **2018**, *172*, 249−261.

(3) Goodman, R. P.; Markhard, A. L.; Shah, H.; Sharma, R.; Skinner, O. S.; Clish, C. B.; Deik, A.; Patgiri, A.; Hsu, Y. H.; Masia, R.; Noh, H. L.; Suk, S.; Goldberger, O.; Hirschhorn, J. N.; Yellen, G.; Kim, J. K.; Mootha, V. K. Hepatic NADH reductive stress underlies common variation in metabolic traits. *Nature* **2020**, *583*, 122−126.

https://doi.org/10.1021/acsomega.3c01688
ACS Omega 2023, 8, 23651−23663

(4) Medina, C. B.; Mehrotra, P.; Arandjelovic, S.; S A Perry, J.; Guo, Y.; Morioka, S.; Barron, B.; Walk, S. F.; Ghesquière, B.; Krupnick, A. S.; Lorenz, U.; Ravichandran, K. S. Metabolites released from apoptotic cells act as tissue messengers. *Nature* **2020**, *580*, 130−135.
(5) Hartl, J.; Kiefer, P.; Kaczmarczyk, A.; Mittelviefhaus, M.; Meyer, F.; Vonderach, T.; Hattendorf, B.; Jenal, U.; Vorholt, J. A. Untargeted metabolomics links glutathione to bacterial cell cycle progression. *Nat. Metab.* **2020**, *2*, 153−166.
(6) Garza, D. R.; Verk, M. C. V.; Huynen, M. A.; Dutilh, B. E. Towards predicting the environmental metabolome from metagenomics with a mechanistic model. *Nat. Microbiol.* **2018**, *3*, 456−460.
(7) Fàbregas, N.; Elena, F. L.; Escámez, D. B.; Tohge, T.; Andújar, C. M.; Albacete, A.; Osorio, S.; Bustamante, M.; Riechmann, J. L.; Nomura, T.; Yokota, T.; Conesa, A.; Alfocea, F. P.; Fernie, A. R.; Delgado, A. I. C. Overexpression of the vascular brassinosteroid receptor BRL3 confers drought resistance without penalizing plant growth. *Nat. Commun.* **2018**, *9*, No. 4680.
(8) Khodadadi, M.; Pourfarzam, M. A. review of strategies for untargeted urinary metabolomic analysis using gas chromatography-mass spectrometry. *Metabolomics* **2020**, *16*, 66−79.
(9) Nipun, T. S.; Khatib, A.; Ibrahim, Z.; Ahmed, Q. U.; Redzwan, I. E.; Primaharinastiti, R.; Saiman, M. Z.; Fairuza, R.; Widyaningsih, T. D.; Al Ajmi, M. F.; Khalifa, S. A. M.; El-Seedi, H. R. GC-MS- and NMR-Based Metabolomics and Molecular Docking Reveal the Potential Alpha-Glucosidase Inhibitors from Psychotria malayana Jack Leaves. *Pharmaceuticals* **2021**, *14*, 978−1006.
(10) Barding, G. A.; Béni, S., Jr.; Fukao, T.; Serres, J. B.; Larive, C. K. Comparison of GC-MS and NMR for Metabolite Profiling of Rice Subjected to Submergence Stress. *J. Proteome Res.* **2013**, *12*, 898−909.
(11) Chen, J.-j.; Liu, Z.; Fan, S.; Yang, D.; Zheng, P.; Shao, W.; Qi, Z.; Xu, X.; Li, Q.; Mu, J.; Yang, Y. T.; Xie, P. Combined Application of NMR- and GC-MS-Based Metabonomics Yields a Superior Urinary Biomarker Panel for Bipolar Disorder. *Sci. Rep.* **2014**, *4*, No. 5855.
(12) Hamade, K.; Fliniaux, O.; Fontaine, J. X.; Molinié, R.; Nnang, E. O.; Bassard, S.; Guénin, S.; Gutierrez, L.; Lainé, E.; Hano, C.; Pilard, S.; Hijazi, A.; El Kak, A.; Mesnard, F. NMR and LC-MS-Based Metabolomics to Study Osmotic Stress in Lignan-Deficient Flax. *Molecules* **2021**, *26*, 767−789.
(13) Liu, Y.; Hong, Z.; Tan, G.; Dong, X.; Yang, G.; Zhao, L.; Chen, X.; Zhu, Z.; Lou, Z.; Qian, B.; Zhang, G.; Chai, Y. NMR and LC/MS-based global metabolomics to identify serum biomarkers differentiating hepatocellular carcinoma from liver cirrhosis. *Int. J. Cancer* **2014**, *135*, 658−668.
(14) Gathungu, R. M.; Kautz, R.; Kristal, B. S.; Bird, S. S.; Vouros, P. The integration of LC-MS and NMR for the analysis of low molecular weight trace analytes in complex matrices. *Mass Spectrom. Rev.* **2020**, *39*, 35−54.
(15) Emwas, A. H. M. The Strengths and Weaknesses of NMR Spectroscopy and Mass Spectrometry with Particular Focus on Metabolomics Research. In *Methods in Molecular Biology*; Elsevier, 2015; Vol. *1277*, pp 161−193.
(16) Beckonert, O.; Keun, H. C.; Ebbels, T. M. D.; Bundy, J.; Holmes, E.; Lindon, J. C.; Nicholson, J. K. Metabolic profiling, metabolomic and metabonomic procedures for NMR spectroscopy of urine, plasma, serum and tissue extracts. *Nat. Protoc.* **2007**, *2*, 2692−2703.
(17) Dona, A. C.; Jimenez, B.; Schafer, H.; Humpfer, E.; Spraul, M.; Lewis, M. R.; Pearce, J. T. M.; Holmes, E.; Lindon, J. C.; Nicholson, J. K. Precision High-Throughput Proton NMR Spectroscopy of Human Urine, Serum, and Plasma for Large-Scale Metabolic Phenotyping. *Anal. Chem.* **2014**, *86*, 9887−9894.
(18) Guo, W.; Jiang, Ch.; Yang, L.; Li, T.; Liu, X.; Jin, M.; Qu, K.; Chen, H.; Jin, X.; Liu, H.; Zhu, H.; Wang, Y. Quantitative Metabolomic Profiling of Plasma, Urine, and Liver Extracts by 1H NMR Spectroscopy Characterizes Different Stages of Atherosclerosis in Hamsters. *J. Proteome Res.* **2016**, *15*, 3500−3510.
(19) Sethi, S.; Pedrini, M.; Rizzo, L. B.; Zeni-Graif, M.; Mas, C. D.; Cassinelli, A. C.; Noto, M. N.; Asevedo, E.; Cordeiro, Q.; Pontes, J. G. M.; Brasil, A. J. M.; Lacerda, A.; Hayashi, M. A. F.; Poppi, R.; Tasic, L.; Brietzke, E. ^{1}H-NMR T_2-edited, and 2D-NMR in bipolar disorder metabolic profiling. *Int. J. Bipolar Disord.* **2017**, *5*, 23−31.
(20) Guleria, A.; Pratap, A.; Dubey, D.; Rawat, A.; Chaurasia, S.; Sukesh, E.; Phatak, S.; Ajmani, S.; Kumar, U.; Khetrapa, C. L.; Bacon, P.; Misra, R.; Kumar, D. NMR based serum metabolomics reveals a distinctive signature in patients with Lupus Nephritis. *Sci. Rep.* **2016**, *6*, No. 35309.
(21) Wagner, L.; Requeni, P. G.; Moazzami, A. A.; Lundh, T.; Vidakovic, A.; Langeland, M.; Kiessling, A.; Pickova, J. ^{1}H NMR-Based Metabolomics and Lipid Analyses Revealed the Effect of Dietary Replacement of Microbial Extracts or Mussel Meal with Fish Meal to Arctic Charr (*Salvelinus alpinus*). *Fishes* **2019**, *4*, 46−68.
(22) Guleria, A.; Misra, D. P.; Rawat, A.; Dubey, D.; Khetrapal, C. L.; Bacon, P.; Misra, R.; Kumar, D. NMR-Based Serum Metabolomics Discriminates Takayasu Arteritis from Healthy Individuals: A Proof-of-Principle Study. *J. Proteome Res.* **2015**, *14*, 3372−3381.
(23) Baranovicová, E.; Galanda, T.; Galanda, M.; Hatok, J.; Kolarovszki, B.; Richterová, R.; Racay, P. Metabolomic profiling of blood plasma in patients with primary brain tumours: Basal plasma metabolites correlated with tumour grade and plasma biomarker analysis predicts feasibility of the successful statistical discrimination from healthy subjects, a preliminary study. *IUBMB Life* **2019**, *71*, 1994−2002.
(24) Ząbek, A.; Stanimirova, I.; Deja, S.; Barg, W.; Kowal, A.; Korzeniewska, A.; Pawiłowicz, M. O.; Baranowski, D.; Gdaniec, Z.; Jankowska, R.; Młynarz, P. Fusion of the 1H NMR data of serum, urine and exhaled breath condensate in order to discriminate chronic obstructive pulmonary disease and obstructive sleep apnea syndrome. *Metabolomics* **2015**, *11*, 1563−1574.
(25) Röhnisch, H. E.; Eriksson, J.; Tran, L. V.; Müllner, E.; Sandström, C.; Moazzami, A. A. Improved Automated Quantification Algorithm (AQuA) and Its Application to NMR-Based Metabolomics of EDTA-Containing Plasma. *Anal. Chem.* **2021**, *93*, 8729−8738.
(26) Emwas, A. H.; Roy, R.; McKay, R. T.; Tenori, L.; Saccenti, E.; Gowda, G. A. N.; Raftery, D.; Alahmari, F.; Jaremko, L.; Jaremko, M.; Wishart, D. S. NMR Spectroscopy for Metabolomics Research. *Metabolites* **2019**, *9*, 123−161.
(27) Lutz, N. W.; Bernard, M. Methodological Developments for Metabolic NMR Spectroscopy from Cultured Cells to Tissue Extracts: Achievements, Progress and Pitfalls. *Molecules* **2022**, *27*, 4214−4239.
(28) Kwon, D. J.; Jeong, H.; Moon, H.; Kim, H. N.; Cho, J. H.; Lee, J. E.; Hong, K. S.; Hong, Y. S. Assessment of green coffee bean metabolites dependent on coffee quality using a 1H NMR-based metabolomics approach. *Food Res. Int.* **2015**, *67*, 175−182.
(29) Hernández-Guerrero, C. J.; Ruano, N. V.; Vallejo, L. G. Z.; Fuentes, A. D. H.; Estrada, K. R.; Lucero, S. Z.; Martínez, D. H.; Martínez, E. B. Bean cultivars (Phaseolus vulgaris L.) under the spotlight of NMR metabolomics. *Food Res. Int.* **2021**, *150*, 110805−110815.
(30) Deborde, C.; Fontaine, J. X.; Jacob, D.; Botana, A.; Nicaise, V.; Forget, F. R.; Lecomte, S.; DecourtiL, C.; Hamade, K.; Mesnard, F.; Moing, A.; Molinié, R. Optimizing 1D ^{1}H-NMR profiling of plant samples for high throughput analysis: extract preparation, standardization, automation and spectra processing. *Metabolomics* **2019**, *15*, 28−39.
(31) Burdziej, A.; Da CostA, G.; Gougeon, L.; Mao, I. L.; Bellée, A.; Costet, M. F. C.; Mérillon, J. M.; Richard, T.; Szakiel, A.; Cluzet, S. Impact of diferent elicitors on grapevine leaf metabolism monitored by ^{1}H NMR spectroscopy. *Metabolomics* **2019**, *15*, 67−77.
(32) Cerulli, A.; Masullo, M.; Pizza, C.; Piacente, S. Metabolite Profiling of "Green" Extracts of Cynara cardunculus subsp. scolymus, Cultivar "Carciofo di Paestum" PGI by ^{1}H NMR and HRMS-Based Metabolomics. *Molecules* **2022**, *27*, 3328−3343.
(33) Tang, F.; Hatzakis, E. NMR-Based Analysis of Pomegranate Juice Using Untargeted Metabolomics Coupled with Nested and Quantitative Approaches. *Anal. Chem.* **2020**, *92*, 11177−11185.
(34) Shen, G.; Huang, Y.; Dong, J.; Wang, X.; Cheng, K. K.; Feng, J.; Xu, J.; Ye, J. Metabolic Effect of Dietary Taurine Supplementation on

https://doi.org/10.1021/acsomega.3c01688
ACS Omega 2023, 8, 23651−23663

Nile Tilapia (Oreochromis niloticus) Evaluated by NMR-Based Metabolomics. *J. Agric. Food Chem.* **2018**, *66*, 368−377.
(35) Matoo, O. B.; Lannig, G.; Bock, C.; Sokolova, I. M. Temperature but not ocean acidification affects energy metabolism and enzyme activities in the blue mussel, Mytilus edulis. *Ecol. Evol.* **2021**, *11*, 3366−3379.
(36) Zotti, M.; Pascali, S. A. D.; Coco, L. D.; Migoni, D.; Carrozzo, L.; Mancinelli, G.; Fanizzi, F. P. ^{1}H NMR metabolomic profiling of the blue crab (Callinectes sapidus) from the Adriatic Sea (SE Italy): A comparison with warty crab (Eriphia verrucosa), and edible crab (Cancer pagurus). *Food Chem.* **2016**, *196*, 601−609.
(37) Angilè, F.; Coco, L. D.; Girelli, C. R.; Basso, L.; Rizzo, L.; Piraino, S.; Stabili, L.; Fanizzi, F. P. ^{1}H NMR Metabolic Profile of Scyphomedusa Rhizostoma pulmo (Scyphozoa, Cnidaria) in Female Gonads and Somatic Tissues: Preliminary Results. *Molecules* **2020**, *25*, 806−824.
(38) Zotti, M.; De Pascali; Del Coco, L.; Migoni, D.; Carrozzo, L.; Mancinelli, G.; Fanizzi, F. P. ^{1}H NMR metabolomic profiling of the blue crab (Callinectes sapidus) from the Adriatic Sea (SE Italy): A comparison with warty crab (Eriphia verrucosa), and edible crab (Cancer pagurus). *Food Chem.* **2016**, *196*, 601−609.
(39) Nanda, M.; Kumar, V.; Arora, N.; Vlaskin, M. S.; Tripathi, M. K. ^{1}H NMR-based metabolomics and lipidomics of microalgae Trends in Plant Science. *Trends Plant Sci.* **2021**, *26*, 984−985.
(40) Arora, N.; Dubey, D.; Sharma, M.; Patel, A.; Guleria, A.; Pruthi, P. A.; Kumar, D.; Pruthi, V.; Poluri, K. M. NMR-Based Metabolomic Approach to Elucidate the Differential Cellular Responses during Mitigation of Arsenic (III, V) in a Green Microalga. *ACS Omega* **2018**, *3*, 11847−11856.
(41) Zhang, W.; Tan, N. G. J.; Li, S. F. Y. NMR-based metabolomics and LC-MS/MS quantification reveal metal-specific tolerance and redox homeostasis in Chlorella vulgaris. *Mol. BioSyst.* **2014**, *10*, 149−160.
(42) Gupta, V.; Thakur, R. S.; Reddy, C. R. K.; Bhavanath, J. Central metabolic processes of marine macrophytic algae revealed from NMR based metabolome analysis. *RSC Adv.* **2013**, *3*, 7037−7047.
(43) Zhang, Y.; Zhang, Z.; Zhao, Y.; Cheng, S.; Ren, H. identifying health effects of exposure to trichloroacetamide using transcriptomics and metabonomics in mice (Mus musculus). *Environ. Sci. Technol.* **2013**, *47*, 2918−2924.
(44) Wang, X.; Liu, L.; Zhang, W.; Zhang, J.; Du, X.; Huang, Q.; Tian, M.; Shen, H. Serum metabolome biomarkers associate low-level environmental perfluorinated compound exposure with oxidative/nitrosative stress in humans. *Environ. Pollut.* **2017**, *229*, 168−176.
(45) Miao, J.; Wang, D.; Yan, J.; Wang, Y.; Teng, M.; Zhou, Z.; Zhu, W. Comparison of subacute effects of two types of pyrethroid insecticides using metabolomics methods. *Pestic. Biochem. Physiol.* **2017**, *143*, 161−167.
(46) Vu, T. H. V.; Lim, H. H.; Shin, H. S. Determination of 15 Biomarkers of Endocrine Disrupting Chemicals in Human Saliva by Gas Chromatography−Mass Spectrometry. *Bull. Korean Chem. Soc.* **2020**, *41*, 424−432.
(47) Del Coco, L.; Vergara, D.; Matteis, S. D.; Mensà, E.; Sabbatinelli, J.; Prattichizzo, F.; Bonfigli, A. R.; Storci, G.; Bravaccini, S.; Pirini, F.; Ragusa, A.; Gardini, A. C.; Bonafè, M.; Maffia, M.; Fanizzi, F. P.; Olivieri, F.; Giudetti, A. M. NMR-Based Metabolomic Approach Tracks Potential Serum Biomarkers of Disease Progression in Patients with Type 2 Diabetes Mellitus. *J. Clin. Med.* **2019**, *8*, 720−739.
(48) Wang, Z.; Lin, Y.; Liang, J.; Huang, Y.; Ma, C.; Liu, X.; Yang. NMR-based metabolomic techniques identify potential urinary biomarkers for early colorectal cancer detection. *J. Oncotarget* **2017**, *8*, 105819−105831.
(49) Emwas, A. H.; Roy, R.; McKay, R. T.; Ryan, D.; Brennan, L.; Tenori, L.; Luchinat, C.; Gao, X.; Zeri, A. C.; Gowda, G. A. N.; Raftery, D.; Steinbeck, C.; Salek, R. M.; Wishart, D. S. Recommendations and Standardization of Biomarker Quantification Using NMR-Based Metabolomics with Particular Focus on Urinary Analysis. *J. Proteome Res.* **2016**, *15*, 360−373.
(50) Lewis, I. A.; Schommer, S. C.; Markley, J. L. rNMR: opensource software for identifying and quantifying metabolites in NMR spectra. *Magn. Reson. Chem.* **2009**, *47*, 123−126.
(51) Robinette, S. L.; Ajredini, R.; Rasheed, H.; Zeinomar, A.; C Schroeder, F.; Dossey, A. T.; Edison, A. S. Hierarchical Alignment and Full Resolution Pattern Recognition of 2D NMR Spectra: Application to Nematode Chemical Ecology. *Anal. Chem.* **2011**, *83*, 1649−1657.
(52) Zhang, F.; Robinette, S. L.; Bruschweiler-Li, L.; Brüschweiler, R. Web server suite for complex mixture analysis by covariance NMR. *Magn. Reson. Chem.* **2009**, *47*, 118−122.
(53) Puig-Castellví, F.; Perez, Y.; Piña, B.; Tauler, R.; Alfonso, I. Comparative analysis of ^{1}H NMR and ^{1}H−^{13}C HSQC NMR metabolomics to understand the effects of medium composition in yeast growth. *Anal. Chem.* **2018**, *90*, 12422−12430.
(54) Chandra, K.; Al-Harthi, S.; Almulhim, F.; Emwas, A. H.; Jaremko, Ł.; Jaremko, M. The robust NMR toolbox for metabolomics. *Mol. Omics* **2021**, *17*, 719−772.
(55) Xia, J.; Psychogios, N.; Young, N.; Wishart, D. S. MetaboAnalyst: a web server for metabolomic data analysis and interpretation. *Nucleic Acids Res.* **2009**, *37*, 652−660.
(56) Meiboom, S.; Gill, D. Modified spin-echo method for measuring nuclear relaxation times. *Rev. Sci. Instrum.* **1958**, *29*, 688−691.
(57) Carr, H. Y.; Purcell, E. M. Effects of diffusion on free precession in nuclear magnetic resonance experiments. *Phys. Rev.* **1954**, *94*, 630−638.
(58) Hwang, T. L.; Shaka, A. J. Water suppression that works. Excitation sculpting using arbitrary waveforms and pulsed field gradients. *J. Magn. Reson., Ser. A* **1995**, *112*, 275−279.
(59) Le Guennec, A.; Tayyari, F.; Edison, A. S. Alternatives to Nuclear Overhauser Enhancement Spectroscopy Presat and Carr−Purcell−Meiboom−Gill Presat for NMR-Based Metabolomics. *Anal. Chem.* **2017**, *89*, 8582−8588.
(60) Smallcombe, S. H.; Patt, S. H.; Keifer, P. A. WET solvent suppression and its applications to LC NMR and high-resolution NMR spectroscopy. *J. Magn. Reson., Ser. A* **1995**, *117*, 295−303.
(61) Ogg, R. J.; Kingsley, R. B.; Taylor, J. S. J. WET, a T_1- and B_1-Insensitive Water-Suppression Method for in Vivo Localized ^{1}H NMR Spectroscopy. *J. Magn. Reson., Ser. B* **1994**, *104*, 1−10.
(62) Hoult, D. I. Solvent peak saturation with single phase and quadrature Fourier transformation. *J. Magn. Reson.* **1976**, *21*, 337−347.
(63) Bax, A. J. A spatially selective composite 90° radiofrequency pulse. *J. Magn. Reson.* **1985**, *65*, 142−145.
(64) Piotto, M.; Saudek, V.; Sklenář, V. Gradient-tailored excitation for single-quantum NMR spectroscopy of aqueous solutions. *J. Biomol. NMR* **1992**, *2*, 661−665.
(65) Liu, M.; Mao, X.; Ye, C.; Huang, H.; Nicholson, J. K.; Lindon, J. C. Improved WATERGATE pulse sequences for solvent suppression in NMR spectroscopy. *J. Magn. Reson.* **1998**, *132*, 125−129.
(66) Simpson, A. J.; Brown, S. A. Purge NMR: Effective and easy solvent suppression. *J. Magn. Reson.* **2005**, *175*, 340−346.
(67) Sklenar, V.; Piotto, M.; Leppik, R.; Saudek, V. Gradient-tailored water suppression for proton-nitrogen-15 HSQC experiments optimized to retain full sensitivity. *J. Magn. Reson., Ser. A* **1993**, *102*, 241−245.
(68) Giraudeau, P.; Silvestre, V.; Akoka, S. Optimizing water suppression for quantitative NMR-based metabolomics: a tutorial review. *Metabolomics* **2015**, *11*, 1041−1055.
(69) Wojtowicz, W.; Zabek, A.; Deja, S.; Dawiskiba, T.; Pawelka, D.; Glod, M.; Balcerzak, W.; Mlynarz, P. Serum and urine ^{1}H NMR-based metabolomics in the diagnosis of selected thyroid diseases. *Sci. Rep.* **2017**, *7*, No. 9108.
(70) Aguilar, J. A.; Nilsson, M.; Bodenhausenbc, G.; Morris, G. A. Spin echo NMR spectra without J modulation. *Chem. Commun.* **2012**, *48*, 811−813.

https://doi.org/10.1021/acsomega.3c01688
ACS Omega 2023, 8, 23651−23663

(71) Baishya, B.; Segawa, T. F.; Bodenhausen, G. Apparent transverse relaxation rates in systems with scalar-coupled protons. *J. Am. Chem. Soc.* **2009**, *131*, 17538−17539.
(72) Zhang, G. Q.; Hirasaki, G. J. CPMG relaxation by diffusion with constant magnetic field gradient in a restricted geometry: numerical simulation and application. *J. Magn. Reson.* **2003**, *163*, 81−91.
(73) Ronczka, M.; Petke, M. M. Optimization of CPMG sequences to measure NMR transverse relaxation time T_2 in borehole applications. *Geosci. Instrum., Methods Data Syst.* **2012**, *1*, 197−208.
(74) Ziener, C.; Kampf, T.; Jakob, P. M.; Bauer, W. R. Diffusion effects on the CPMG relaxation rate in a dipolar field. *J. Magn. Reson.* **2010**, *202*, 38−42.
(75) Aranı, N.; Ott, K. H.; Roongta, V.; Mueller, L. Metabolomic analysis using optimized NMR and statistical methods. *Anal. Biochem.* **2006**, *355*, 62−70.
(76) Ernst, R. R.; Anderson, W. A. Application of Fourier Transform Spectroscopy to Magnetic Resonance. *Rev. Sci. Instrum.* **1966**, *37*, 93−102.
(77) Freeman, R.; Hill, H. D. W. Phase and Intensity Anomalies in Fourier Transform NMR. *J. Magn. Reson.* **1971**, *4*, 366−383.
(78) Turner, C. J.; Hutton, W. C. Suppression of Artifacts in Phase-Sensitive COSY. *J. Magn. Reson.* **1992**, *100*, 469−483.
(79) Bain, A. D.; Burton, I. W.; Reynolds, W. F. Artifacts in two-dimensional NMR. *Prog. Nucl. Magn. Reson. Spectrosc.* **1994**, *26*, 59−89.
(80) Al-Nemi, R.; Makki, A. A.; Sawalha, K.; Hajjar, D.; Jaremko, M. Untargeted Metabolomic Profiling and Antioxidant Capacities of Different Solvent Crude Extracts of Ephedra foeminea. *Metabolites* **2022**, *12*, 451−481.
(81) Ząbek, A.; Ochab, M. K.; Jawień, E.; Młynarz, P. Biodiversity in targeted metabolomics analysis of filamentous fungal pathogens by ^{1}H NMR-based studies. *World J. Microbiol. Biotechnol.* **2017**, *33*, 132−143.
(82) Szczepski, K.; Al-Younis, I.; Dhahri, M.; Lachowicz, JI; Al-Talla, ZA.p; Almahasheer, H.; Alasmael, N.; Rahman, M.; Emwas, A. H.; Jaremko, Ł.; Jaremko, M. Metabolic biomarkers in cancer. *Metabolomics* **2023**, *1*, 173−198.
(83) Emwas, A. H.; Szczepski, K.; Poulson, B. G.; McKay, R.; Tenori, L.; Saccenti, E.; Lachowicz, J.; Jaremko, M. Nuclear magnetic resonance in metabolomics. *Metabolomics Perspectives* **2022**, 149−218.
(84) Chandra, K.; Al-Harthi, S.; Sukumaran, S.; Almulhim, F.; Emwas, A. H.; Atreya, H. S.; Jaremko, Ł.; Jaremko, M. NMR-based metabolomics with enhanced sensitivity. *RSC Adv.* **2021**, *11*, 8694−8700.
(85) Salem, M. A.; Jüppner, J.; Bajdzienko, K.; Giavalisco, P. Protocol: a fast, comprehensive and reproducible one-step extraction method for the rapid preparation of polar and semi-polar metabolites, lipids, proteins, starch and cell wall polymers from a single sample. *Plant Methods* **2016**, *12*, No. 45.
(86) Dghaim, R.; Hammami, Z.; Al Ghali, R.; Smail, L.; Haroun, D. The Mineral Composition of Date Palm Fruits (*Phoenix dactylifera* L.) under Low to High Salinity Irrigation. *Molecules* **2021**, *26*, 7361−7374.
(87) Vayalil, P. Date Fruits (*Phoenix dactylifera* Linn): An Emerging Medicinal Food. *Food Sci. Nutr.* **2012**, *52*, 249−271.
(88) Robosky, L. C.; Reily, M. D.; Avizonis, D. Improving NMR sensitivity by use of salt-tolerant cryogenically cooled probes. *Anal. Bioanal. Chem.* **2007**, *387*, 529−532.

https://doi.org/10.1021/acsomega.3c01688
ACS Omega 2023, 8, 23651−23663